Development of Fully Implantable Retinal Prosthesis with 3-Dimensionally Stacked LSI

Tetsu Tanaka

Professor
Department of Biomedical Engineering, Graduate School of Biomedical Engineering
E-mail: ttanaka@bme.tohoku.ac.jp

Abstract

To restore visual sensation of blind patients, we have proposed and developed a fully implantable retinal prosthesis with 3-dimensionally stacked retinal prosthesis chip. The retinal prosthesis chip consists of several LSI chips that are vertically stacked and electrically connected by using 3-D integration technology. Our retinal prosthesis chip has small size, light weight, and high resolution, which leads to high quality of life (QOL) to the patients.

In this study, we fabricated various kinds of stimulus electrodes with different sizes and materials, and verified low impedance characteristics with porous materials such as Pt-b and TiN. And also, we developed electric connection technique between retinal prosthesis chip and flexible cable. Moreover, we fabricated and evaluated coils for power transmission between extra- and intraocular units in the fully implantable retinal prosthesis. Additionally, we fabricated Si neural probe for recording of neural action potentials from the visual cortex of brain.

1. Introduction

Recently, with a progress of an aging society, the number of blind patients has been remarkably increasing in the world. In particular, a lot of people lose their vision due to the ocular diseases such as cataract and glaucoma in developing countries, because medical treatments have not progressed. These ocular diseases can be cured by present medical technologies. On the other hand, effective medical cures for retinal diseases such as retitinitis pigmentosa (RP) and age-related macular degeneration (AMD) have not been established yet. And also, more than 10 million people are blind due to these retinal diseases in the world. Photoreceptor cells in the retina have a very important role and convert incident light signals into electrical signals. In the retina of blind patients with RP or AMD, photoreceptor cells are almost or sometimes completely absent. This results in the loss of sight. However, in most cases, retinal cells such as bipolar cells and ganglion cells often remain even in blind patients with RP and AMD, and it was confirmed that a light perception can be elicited by electrical stimulation to remaining visual pathway [1]. Considering this situations, it will be possible to restore one's visual sensation with stimulating the remaining retinal cells. In recent years, several visual prostheses have been developing [2,3]. We have also developed a fully implantable retinal prosthesis with a three-dimensionally (3D) stacked LSI [4-6].

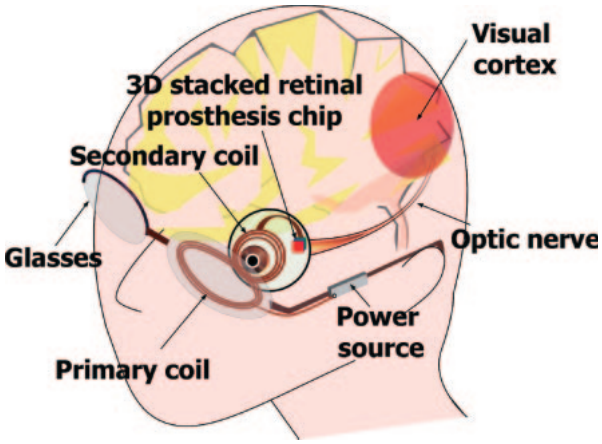

Fig. 1. Concept of fully implantable retinal prosthesis.

Figure 1 shows a conceptual drawing of our fully implantable retinal prosthesis. The implantable retinal prosthesis is composed of the extraocular and the intraocular devices, which are connected by a telemetric inductive link. The extraocular devices consist of a primary coil and a transmitter for power transmission. The intraocular device consists of the 3D stacked retinal prosthesis chip, a flexible cable with a stimulus electrode array, and a secondary coil for power reception. The 3D stacked retinal prosthesis chip is attached to the surface of the FPC which has a stimulus electrode array on the backside. In the 3D stacked retinal prosthesis chip, photodetector layer, image processing circuit layer, and stimulus current generator circuit layer are vertically stacked and electrically connected by many through Si via (TSV) formed in Si substrate. By implanting the 3D stacked retinal prosthesis chip into the eyeball, the patients can employ their own lens and cornea, and can shift a gaze point by moving the eyeball, leading to high speed visual information processing by using saccadic effects. As the 3D stacked retinal prosthesis chip has layered structure similar to human retina, photodetectors with more than 1000 pixels can be fabricated in the retinal chip. This leads to small chip size, light weight, large fill-factor, high resolution, and the resultant high QOL.

In this paper, we studied materials of flexible cable with stimulus electrode array for retinal prosthesis module. We also investigated electrical characteristics of various kinds of stimulus electrode, micro bumps for electric connection between retinal prosthesis chip and flexible cable, and power transmission characteristics with coils. Moreover, we studied Si neural probe for recording of neural action potentials from the visual cortex of brain.

2. Evaluation of the Flexible Cable Material

As the flexible cable is attached to retina directly, there are several requirements for the flexible cable material. First, the material needs biocompatibility to prevent retina from being denatured. Low percentages of water absorption are also necessary for the flexible cable. Increase of flexible cable's volume due to absorption of water might lead to short-interconnections. Moreover, flexibility is necessary in order to fix the flexible cable along the eyeball.

To meet these requirements, we examined both polyimide and parylene C for the flexible cable material. These are polymers having biocompatibility and high flexibility. Especially, parylene C has United States Pharmacopoeia (USP) Class VI status [7]. We evaluated the time dependence of water absorption for both polyimide film and parylene C film. Polyimide film and parylene C film deposited on 4-inch wafer with the thickness of 5-μm was soused in water, and weight variation was measured in every given period of time. The result is shown in Fig. 2.

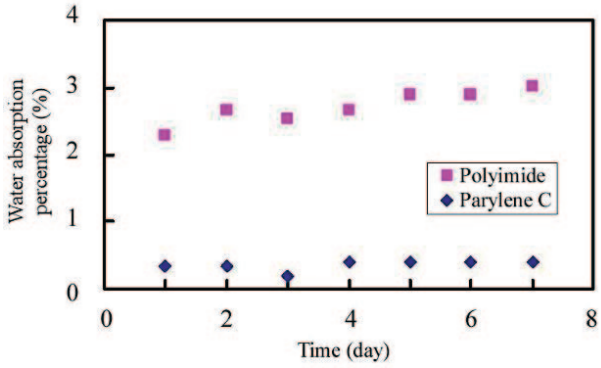

Fig. 2. Time dependence of the percentage of water absorption for polyimide and parylene C.

The water absorption percentage of parylene C is lower than 0.5 % as shown in Fig. 2. On the other hand, the percentage of water absorption of polyimide is higher than 3 % after 7 days. Therefore, parylene C is more suitable than polyimide for the flexible cable material.

We fabricated a flexible cable using these polymers. These flexible cables were fabricated on a 2-inch Si wafer covered with thermally grown SiO_2 by using standard photolithographic techniques. First, 3-μm-thick polymer was formed on the SiO_2 and holes for stimulus electrodes were formed in the film by conventional reactive ion etching (RIE). Then, holes were filled with Pt by lift-off technique. After Au/Cr wirings were formed by wet etching, the Au/Cr wirings were covered with the 17-μm-thick polymer. Finally, the Si wafer was immersed in buffered HF solution to separate the flexible cable from the Si wafer by SiO_2 etching between the polymer and the wafer. The flexible cable with parylene C was fabricated, as shown in Fig. 3. It is confirmed that the retinal prosthesis cable can be successfully formed with parylene C.

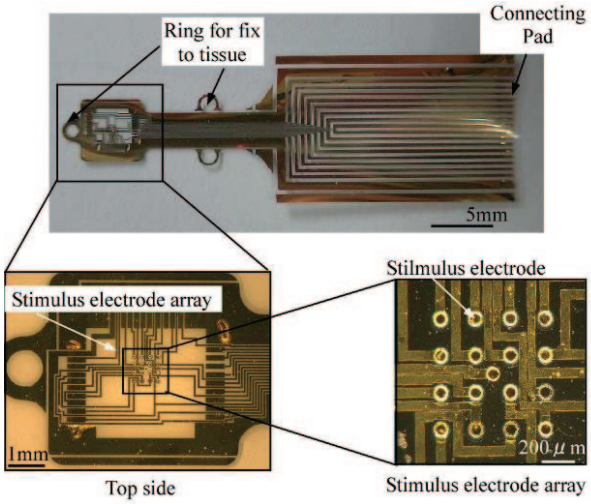

Fig. 3. Photographs of the fabricated flexible cable using parylene C.

3. Evaluation of the Stimulus Electrode Material

As the stimulus electrode is used to stimulate ganglion cells in retina, it is attached to living tissue, as well as flexible cable. Therefore, the stimulus electrode material needs biocompatibility. In addition, because many stimulus electrodes are necessary to obtain visual sensation with high resolution, the size of stimulus electrode should be small. Moreover, the impedance between the stimulus electrode and retina cells needs to be low in order to stimulate the retina cell effectively.

We examined three materials for stimulus electrode; Al, Pt-b, TiN. To investigate the impedance of each material, we fabricated stimulus electrode series, as shown in Fig. 4.

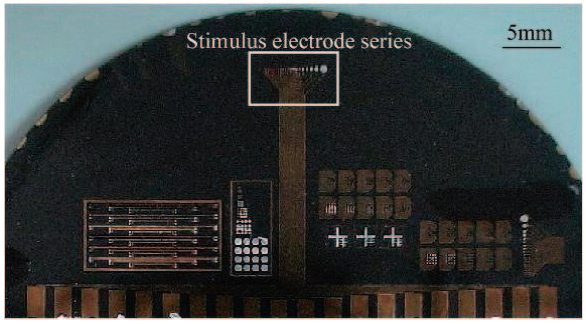

Fig. 4. Photographs of the fabricated stimulus electrode series.

This stimulus electrode series includes 20 types of stimulus electrode size; 5, 7.5, 10, 12.5, 15, 20, 25, 30, 40, 50, 60, 70, 80, 90, 100, 125, 150, 200, 300, and 500 µm. The stimulus electrode series was fabricated on a 2-inch Si wafer by using standard photolithographic techniques. First, a 15-µm-thick polyimide film was formed on the Si wafer. Second, Al wirings were formed by wet etching. Then, stimulus electrode of each material was formed by lift-off technique except Al electrode. Finally, the Al wirings were covered with a 3-µm-thick photosensitive polyimide and formed holes for the stimulus electrode by using photolithographic technique. Figure 5 shows results of laser microscopy analysis of Pt-b and TiN electrode. Figure 6 shows photomicrograph of Pt-b and TiN electrode.

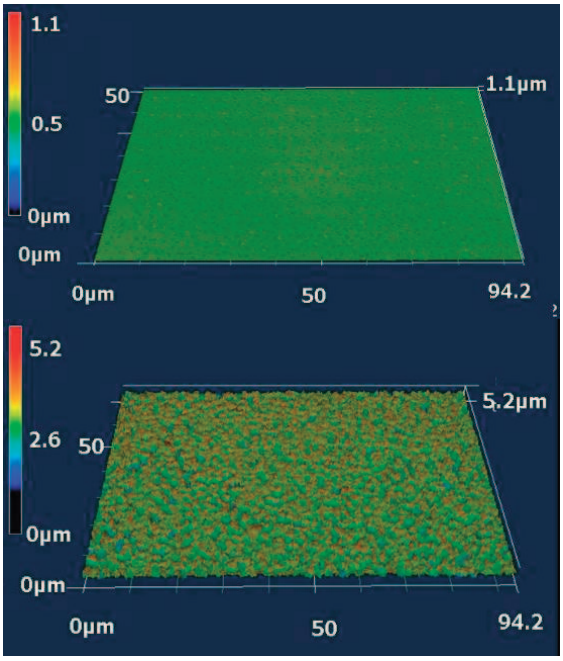

Fig. 5. Resultof laser microscopy analysis of Pt-b and TiN electrode.

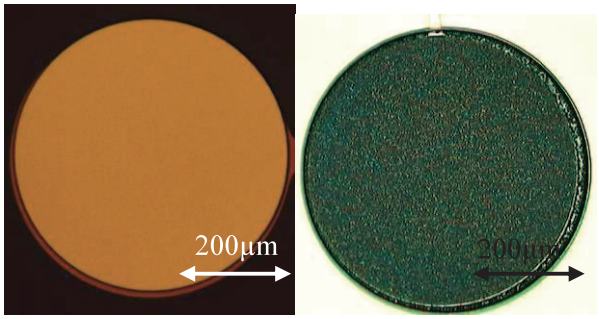

Fig. 6. Photomicrograph of Pt-b and TiN electrode.

In order to characterize the interface between the stimulus electrodes and electrolyte, we measured electrical impedance of the fabricated stimulus electrodes with an impedance analyzer (Solartron 1260, U.K.). Measurements were performed with the frequency ranging from 10 Hz to 1 MHz using the 10 mV AC sine signal in 0.9 % saline solution. Ag/AgCl electrode and Pt electrode were employed as a reference electrode and counter electrode, respectively.

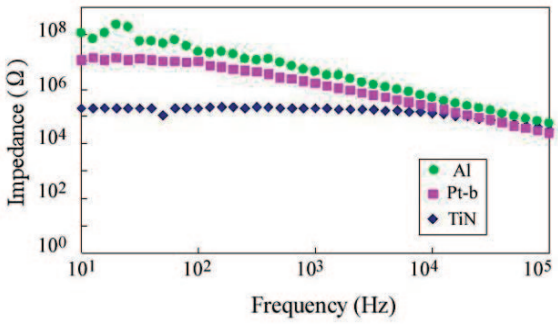

Fig. 7. Impedance spectra of Al, Pt-b and TiN stimulus electrodes.

Figure 7 shows the dependence of impedance on frequency for each material with the stimulus electrode size of 50 µm. The Al, Pt-b, and TiN stimulus electrodes had the impedance of 4.15 MΩ, 1.66 MΩ and 197 kΩ at 1 kHz, respectively. As shown in Fig. 5, Pt-b electrode has high asperity surface, which reduces impedance value of Pt-b electrode. On the other hand, because of electrochemical characteristics of TiN, TiN electrode has lower impedance value despite its smooth surface. Therefore, by increasing asperity of TiN electrode surface, stimulus electrodes with extremely low impedance might be obtained.

4. Fabrication Technique of Micro Bump on Flexible Substrate

We have successfully fabricated the implantable retinal prosthesis in which both retinal prosthesis chip and flexible cable was connected by wire bonding. However, electric connection using wire bonding increase an area of retinal prosthesis chip when number of pixels increase with the objective of high resolution. Moreover, electric connection using wire bonding cannot improve advantages of 3D stacked retinal prosthesis chip. To overcome this problem, we developed electric connection technique between retinal prosthesis chip and flexible cable using micro bump as shown in Fig. 8.

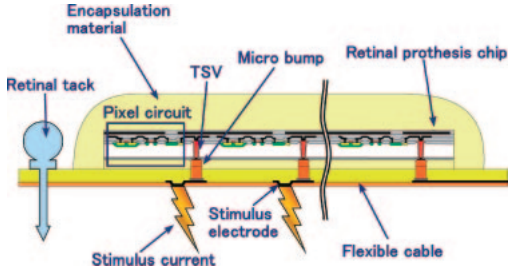

Fig. 8. Cross-sectional view of 3D stacked retinal prosthesis chip and flexible cable.

Figure 9 shows fabrication process flow of micro bump. Thick polyimide film was employed as flexible substrate, and wirings were fabricated by patterning of Al layer evaporated on polyimide substrate. The micro bump made of In/Au was fabricated by lift-off technique. First, thick resist film for lift-off was spin-coated, and Al layer for hard mask of resist etching was evaporated. Then, after Al layer patterning, Al wirings under thick resist film was exposed by O_2-RIE. Finally, In/Au micro bump was formed by evaporation and lift-off technique. Figure 10 shows photomicrograph of fabricated In/Au micro bump with 5-μm-width and 5-μm-height. As shown in this figure, micro bump was successfully fabricated.

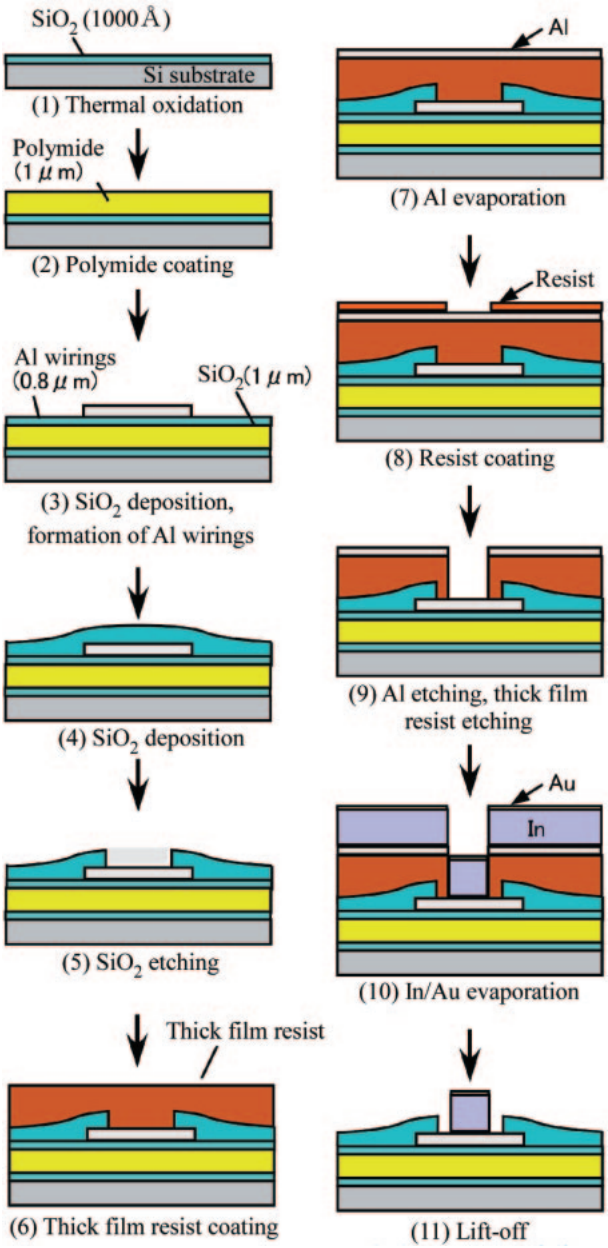

Fig. 9. Fabrication process flow of micro bump.

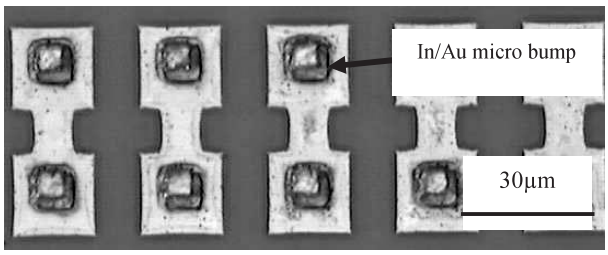

Fig. 10. Photomicrograph of fabricated In/Au micro bump on flexible substrate.

5. Fabrication of Secondary Coil for Power Supply

In our fully implantable retinal prosthesis system, we employ electromagnetic induction as a power delivery method, which means an inductive type power supply to the 3D retinal prosthesis chip, to prevent the eyeball from being infected as shown in Fig. 11. This power delivery system is composed of a primary coil, an extraocular power supply circuit, a secondary coil, and an RF/DC voltage conversion chip for converting AC voltage to DC voltage, as shown in Fig. 12. Several papers have been reported the power supply system, which were used a copper wire for 2nd inductive coil in the eyeball. However, these approaches have possibility to infect the eyeball during and after the surgical operation, if the copper wired inductor size is larger to increase power transmission. In this paper, we proposed new power delivery method using a downsized Cu thin film inductor as a 2nd coil, which can minimize risks of the eyeball being infection diseases. We also evaluated the frequency characteristics of Cu thin film inductor.

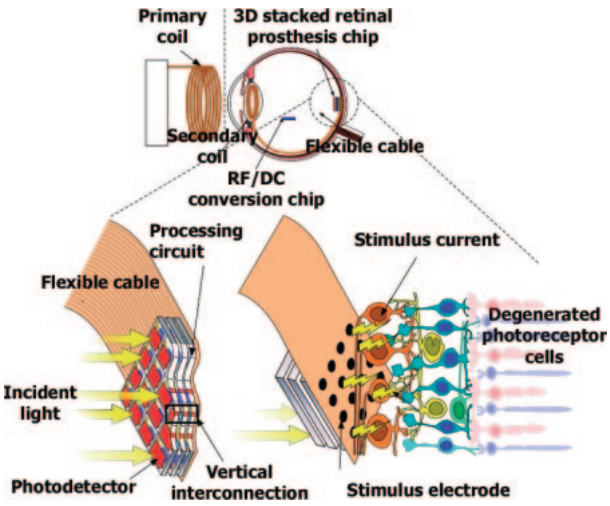

Fig. 11. Configuration of fully implantable retinal prosthesis system with 3D stacked retinal prosthesis chip.

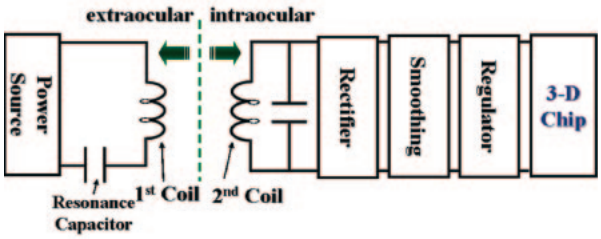

Fig. 12. Circuit diagram of extraocular and intraocular units.

In order to operate the 3D retinal prosthesis chip properly, it is necessary for the 2nd coil to have high inductive performance. Figure 12 shows a circuit diagram of power delivery including two electromagnetic inductors in both extra- and intra-ocular unit. With increasing the turn number of 2nd coil, mutual inductance and the resultant transmitted voltages are increasing. We investigated the effective power transmission to operate the 3D retinal chip by implanted a crystalline lens to the eyeball.

Several types of inductors were fabricated with a line width of 10μm and a line thickness of 1μm. These inductors have various turn numbers of 3.5, 5.5 and 7.5. In order to enhance the coil permeability, the FePt-MND (Magnetic Nano-dot) layer with the thickness of 100nm was formed on SiO2 layer by self-assembled nano-dot deposition (SAND) method, where FePt and SiO2 were co-sputtered in high vacuum RF magnetron sputtering equipment. A fabrication process flow of our spiral inductor with magnetic MND layer is shown in Fig. 13. Firstly, the spiral pattern was formed on a SiO_2 isolation layer by using I-line photolithographic techniques. The FePt MNDs with 100 nm in thickness were formed in the SiO_2 film by a SAND method where FePt and SiO_2 were co-sputtered in a high vacuum RF magnetron sputtering equipment. To enhance the electromagnetic permeability, thermal annealing was performed at 600 °C. To form a shape of spiral in the FePt MND layer, Ar ion milling was used for MND layer etching, and continuously, the SiO_2 layer was etched by using a CF_4/H_2 etching process. For electrical isolation between FePt MND layer and Cu spiral patterns, we formed a passivation oxide layer by plasma tetraethylorthosilicate (TEOS) chemical vapor deposition (CVD). Then, Cu spiral strip was formed out by EP Cu and the subsequent chemical mechanical polishing (CMP) planarization technique. Then we used aluminum as an interconnection. To investigate the effect of FePt MND layer on the characteristics of spiral inductors, we fabricated the inductors without MND layer, which we called the standard inductor. The inductances characteristics were evaluated under various frequency conditions. And also we simulated the Cu spiral inductor model at the same conditions to evaluate the experimental validation by using high frequency electromagnetic simulator.

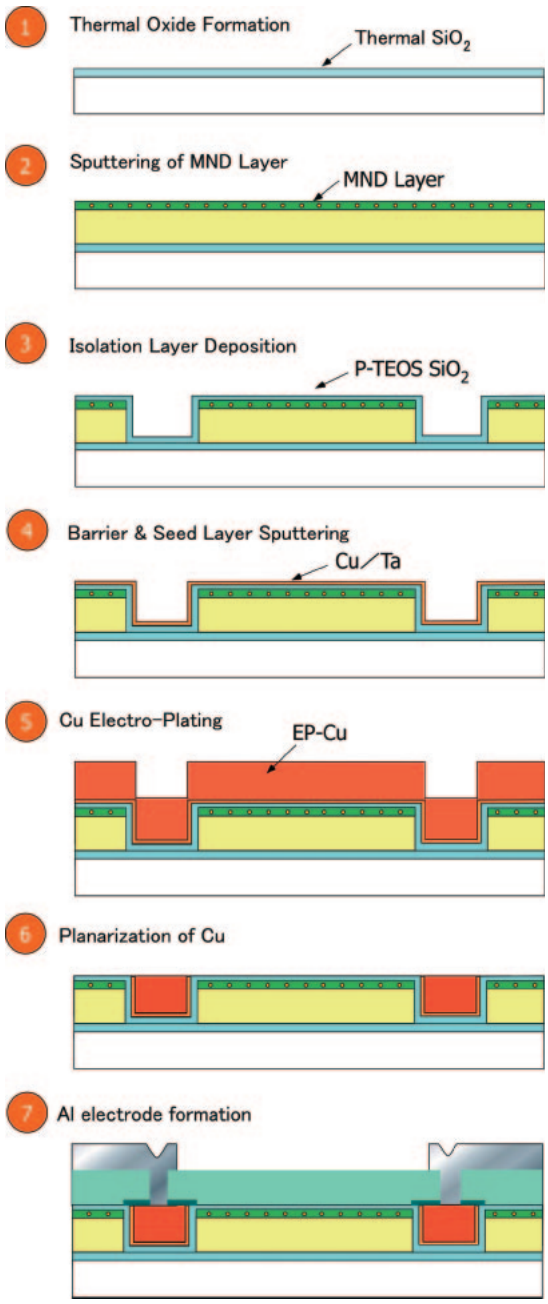

Fig. 13. Process flow of Cu spiral inductor with MND layer fabrication.

The photograph of fabricated Cu spiral inductor with a FePt MND layer is shown in Fig. 14. Figure 15 shows a cross-sectional SEM image of the fabricated Cu spiral inductor with a FePt MND layer. This figure corresponds to 8th process step in Fig. 13. The FePt MND layer was clearly observed in this figure although the Cu strips were slightly dished by CMP process in an overall wafer.

Figure 16 shows the frequency dependence of inductance values. The thin film inductors show the inductance values with ranges of 6 nH to 23 nH and high quality-factor of 3. The roll-off of inductance values at the frequencies from 1 GHz to 4 GHz seems to be associated with LC resonance [8]. It is clearly indicated that an effectiveness of inductance property

as to increase inner areas in the inductor and resistances of internal Cu thin film. We successfully fabricated the Cu thin film type inductors with high inductance performance for the power transmission.

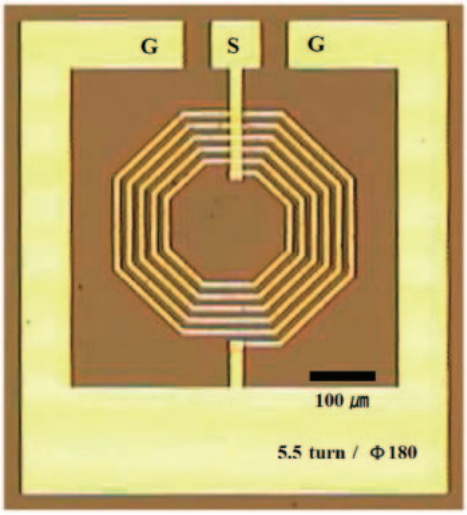

Fig. 14. Photograph of fabricated Cu spiral inductor with FePt-MND layer.

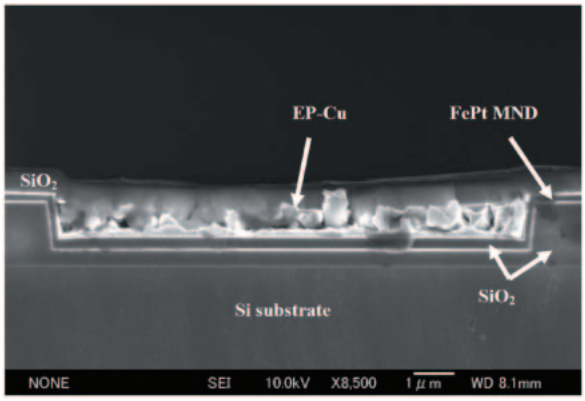

Fig. 15. SEM image of a cross-sectional view of the fabricated Cu spiral inductor with FePt-MND layer.

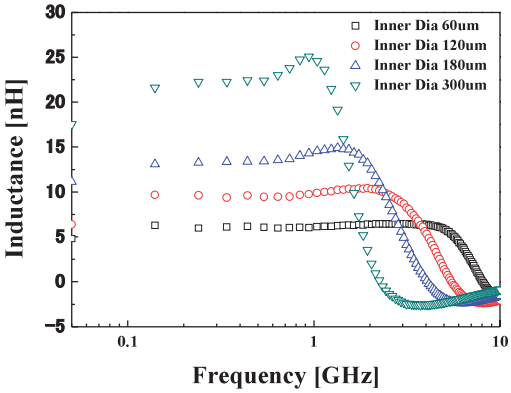

Fig. 16. Frequency characteristics of Cu thin film inductors. The coils have number of winding, N=5.5.

6. Development of Si Neural Probe with Microfluidic Channel

In animal experiments using our retinal prosthesis, we measure neuronal activity in visual cortex of brain by Si neural probe. We have successfully fabricated Si neural probe which has recording sites on both front- and back-side of Si. In this paper, we studied Si neural probe with microfluidic channel for the purpose of injection of neurotransmitter such as a glutamate into the brain

The recording of neural action potentials is the principal technique to understand the neural systems. A Si neural probe is one of the most important tools for the recording [9-14]. By adding the drug delivery functions to Si neural probe, we can record neuronal signals when drugs are injected around neurons. And also, it is possible to apply Si neural probe to Drug Delivery System. Drug Delivery System (DDS) is the system which controls drug distributions in a body quantitatively, spatially, and temporally. The DDS will make it possible to increase drug effect while reducing drug side effect. This kind of Si neural probes will be useful in treatment of brain diseases by transporting drugs into the brain depths. These functions can be realized by integrating microfluidic channels with the neural probe.

Figure 17 illustrates the designed Si probe with microfluidic channel. The microfluidic channel was formed by using wafer direct bonding techniques. Two wafers were bonded by not an adhesive but a covalent bonding of atoms [15].

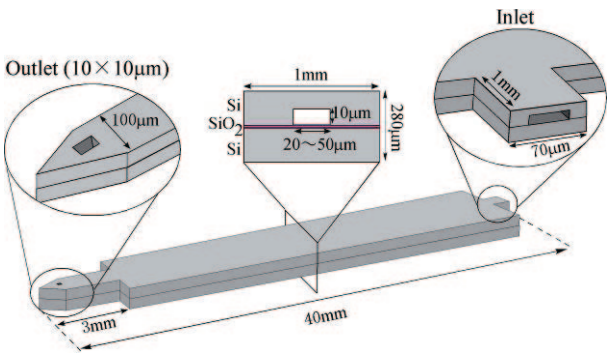

Fig. 17. Design of the Si neural probe with microfluidic channel.

This Si probe has the length of 40 mm and the width of 1 mm and the thickness of 280 μm. A tip of the Si probe has the length of 3 mm and the width of 100 μm. In this Si probe, microfluidic channel with the width of 20~50 μm and the depth of 10 μm is formed. And the outlet of microfluidic channel is formed at the tip with the size of 10 × 10 μm^2. The inlet of microfluidic channel is formed at the end of the Si probe, with the size of 200~500 μm^2 large. The fabrication sequence of our Si probe is illustrated in Fig. 18. At first, we formed the grooves on a Si wafer surface by using D-RIE. The

etched micro grooves have the depth of 10 μm. Then, we rinsed this processed wafer by standard clean 1 (SC-1), and the wafer surface was covered by thin oxidized layer. On another wafer, a thermal oxidized layer with the thickness of 300 nm was formed. When we stack two wafers, hydrogen bonds are formed. By annealing stacked wafers, hydrogen bonds changed to covalent Si-O bonds accordingly with the reaction below:

$$\equiv SiOH + OHSi \equiv \leftrightarrow Si - O - Si + H_2O. \quad (1)$$

Therefore, the bonding strength is increased. Finally, the Si probe was etched off from the wafer by D-RIE.

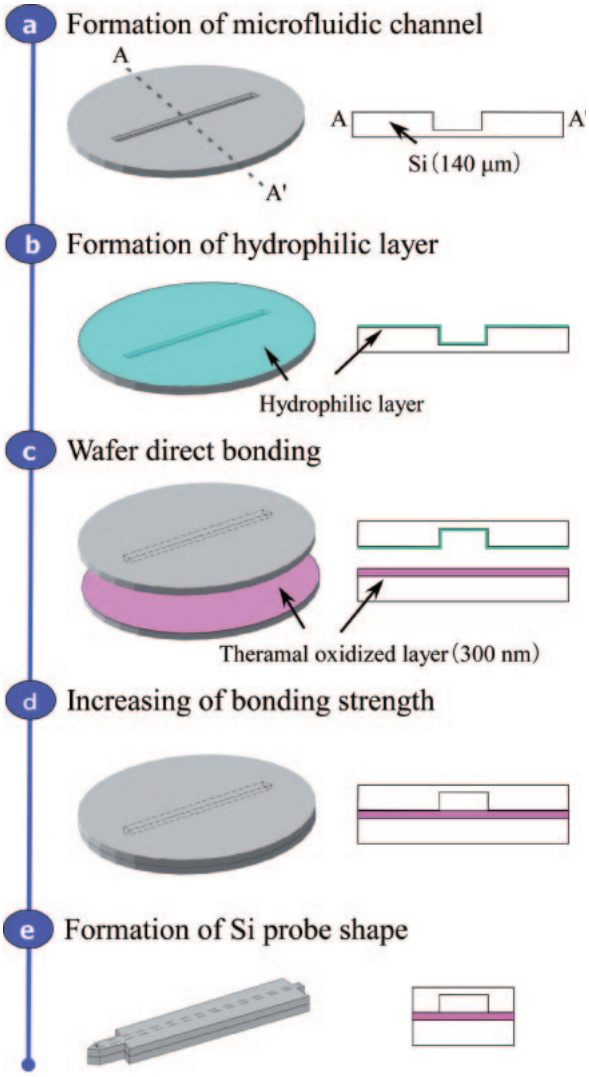

Fig. 18. Fabrication sequence of the Si neural probe with microfluidic channel.

Figure 19 shows the overall structure of the fabricated Si probe. From this picture, we observed that the fluidic outlet was successfully formed. The cross-sectional SEM image of the fabricated microfluidic channel is shown in Fig. 20. We confirmed that the two wafers were completely bonded by the wafer direct bonding.

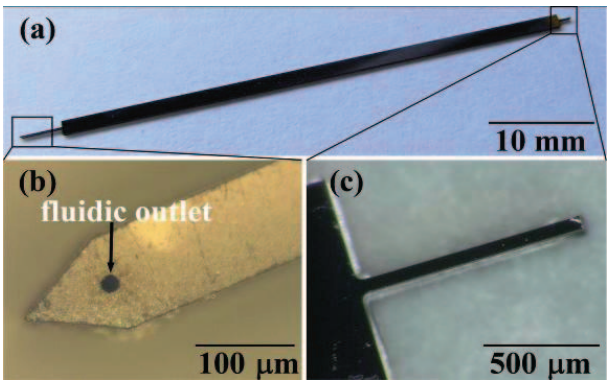

Fig. 19. Photograph of the fabricated Si neural probe. (a) Overall view of the fabricated Si probe, (b) Outlet of the Si probe, (c) Inlet of the Si probe.

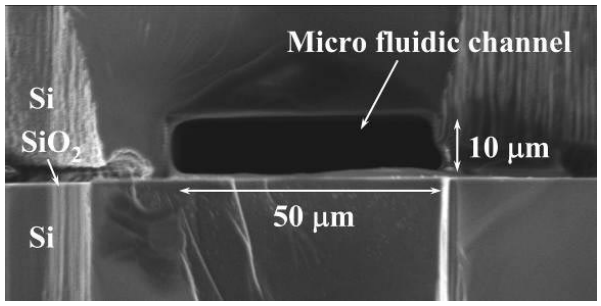

Fig. 20. SEM picture of the cross sectional area of the fabricated Si neural probe.

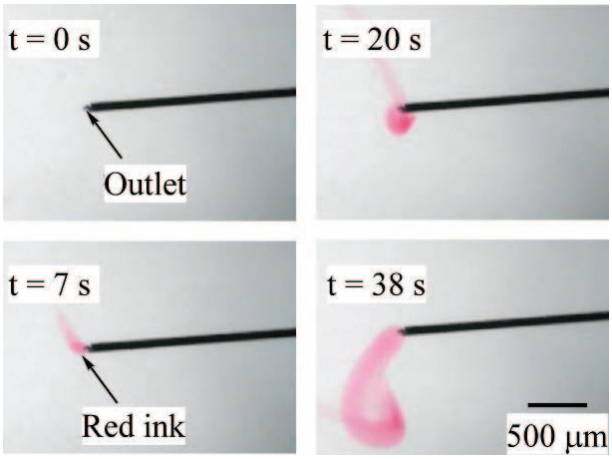

Fig. 21. Ejection of the red ink from the fluidic outlet.

The fluidic experimental system consists of a syringe pump and a pressure meter. At first, we confirmed the strength of the fluidic channel. In the experiment, we injected red ink into the fluidic channel with flow pressure of 1000 mmHg. Figure 21 shows the ejection of red ink from the fluidic outlet. From this experiment, it is confirmed that the microfluidic channel has enough strength to inject fluidic medicine.

We also evaluated relationships between the flow rate and the pressure drop through microfluidic channel. We changed a flow rate from 0.1 to 0.4 μl/min with the

syringe pump, and we measured the pressure drop across the channel by the pressure meter. We recorded the fluidic characteristics of microfluidic channel, and compared with theoretical calculations. The pressure drop (Δp) is defined as:

$$\Delta p = \frac{\mu V (Re \times f) L}{2D^2} \qquad (2)$$

where μ is the viscosity of fluid (~8.9×10^{-4} kg/ms at 25 °C for water), Re × f is the product of the Reynolds number and the Darcy friction factor (~64 in laminar flow), L is the length of the channel (40 mm), and D is the hydraulic diameter of the channel as defined by

D = 4 × (Cross-sectional area / wetted perimeter). (3)

As shown in Fig. 22, the measured values agree well with the theoretical calculations.

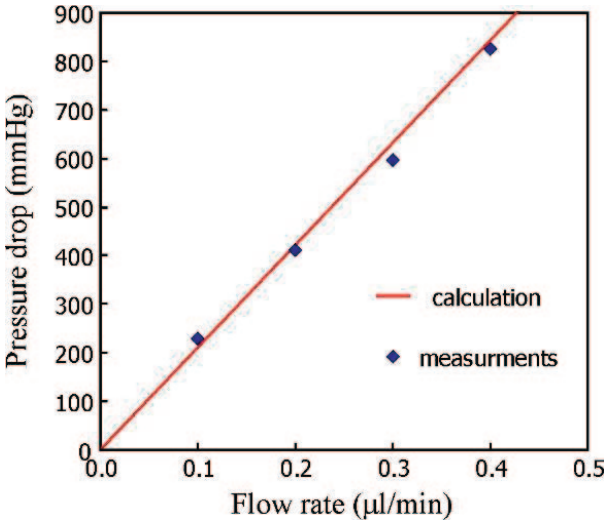

Fig. 22. Relationship between the flow rate and the pressure drop through microfluidic channel.

7. Conclusion

We reported progress in development of Fully Implantable Retinal Prosthesis with 3-Dimensionally Stacked LSI. We examined both polyimide and parylene C for the flexible cable material, and fabricated the flexible cable using these polymers. The water absorption percentage of parylene C is lower than 0.5 %. We also examined Al, Pt-b, and TiN for stimulus electrodes. The Impedance of TiN stimulus electrode was 197 kΩ, which is the lowest among three materials. Additionally, we developed fabrication sequence of micro bump for electric connection between retinal prosthesis chip and flexible cable. We also fabricated the Cu thin film inductors with high inductance performance for the 3-D retinal prosthesis system. Inductance value of 23nH is proven enough possibility to apply the Cu thin film inductor for an implantable retinal prosthesis system. In addition, we successfully obtained the resonance frequency at 4 GHz, which is due to the design of inductors. Based on results, we assume that the Cu thin film inductor can be available as a power delivery system for low power and high data transmission speed. Furthermore, we successfully fabricated the Si neural probe with microfluidic channel. From the ejection test, we confirmed that the Si probe had the sufficient large bonding strength to inject drugs. Additionally, we measured the pressure drop in the microfluidic channel. The measured value agreed well with the theoretical calculations which indicated the fabricated microfluidic channel shapes fitted as we designed. Through this work, we established the fabrication method of microfluidic channel into Si neural probe which is used as the component of the intelligent Si neural probe.

Acknowledgements

The author acknowledges the support of Tohoku University Global COE Program "Global Nano-Biomedical Engineering Education and Research Network Centre". This work was performed in Micro/Nano-Machining Research and Education Center, Tohoku University.

References

[1] Medeiros NE and Curcio CA. Preservation of ganglion cell layer neu-rons in age-related macular degeneration. *Investigative Ophthalmology & Visual Science* **42**, 795-803, 2001.

[2] Humayun MS, Juan E, Weiland JE, Dagnelie G, Katona S, Greenberg R, and Suzuki S. Pattern electrical stimulation of the human retina. *Vision Research* **39**, 2569-2576, 1999.

[3] Ohta J, Yoshida N, Kagawa K, and Nunoshita M. Proposal of application of pulsed vision chip for retinal prosthesis. *Japanese Journal of Applied Physics* **41**, 2322-2325, 2002.

[4] Kurino H, Lee KW, Nakamura T, Sakuma K, Park KT, Miyakawa N, Shimazutsu H, Kim KY, Inamura K, and Koyanagi M. Intelligent image sensor chip with three dimensional structure. *International Electron Devices Meeting Technical Digest*, 879-882, 1999.

[5] Koyanagi M, Nakagawa Y, Lee KW, Nakamura T, Yamada Y, Inamura K, Park KT, and Kurino H. Neuromorphic vision chip fabricated using three-dimensional integration technology. *International Solid-State Circuit Conference Digest of Technical Papers*, 270-271, 2001.

[6] Tanaka T, Sato K, Komiya K, Kobayashi T, Watanabe T, Fukushima T, Tomita H, Kurino H, Tamai M, and Koyanagi M. Fully Implantable Retinal Prosthesis Chip with Photodetector and Stimulus Current Generator. *International Electron Devices Meeting Technical Digest*, 1016-1017, 2007.

[7] Rodger DC, Weiland JD, Humayun MS, and Tai YC. Scalable high lead-count parylene package for retinal prostheses. *Sensors and Actuators B: Chemical,* **117**, 107-114, 2006.
[8] Shin DH, Kim CS, Jeong JH, Bae S, Nam SE, and Kim HJ. Effect of magnetic anisotropy on the current capability of thin film inductor. *J Appl Phys* **87**, 5852-5854, 2000.
[9] Drake KL, Wise KD, Farraye J, Anderson DJ, and Bement L. Performance of planar multisite microprobes in recording extracellular single-unit intracortical activity. *IEEE Transactions on Biomedical Engineering* **35**, 719-732, 1988.
[10] Wise KD, Anderson DJ, Hetke JF, Kipke DR, and Najafi K. Wireless Implantable Microsystems: Electronic Interface to the Nervous System. *Proceedings of the IEEE, Special Issue on Biomedical Applications for MEMS and Microfluidics* **92**, 76-97, 2004.
[11] Campbell PK, Jones KE, Huber RJ, Horch KW, and Normann RA. A silicon-based, three-dimensional neural interface: manufacturing processes for an intracortical electrode array. *IEEE Transactions on Biomedical Engineering* **38**, 758-768, 1991.
[12] Kewleya DT, Hillsb MD, Borkholderb DA, Oprisb IE, Malufb NI, Stormentb CW, Bowera JM, and Kovacsb GTA. Plasma-etched neural probes. *Sensors and Actuators A: Physical* **58**, 27-35, 1997.
[13] Kovacs GTA, Storment CW, Halks-Miller M, Belczynski CR, Santina CCD, Lewis ER, and Maluf NI. Silicon-substrate microelectrode arrays for parallel recording of neural activity in peripheral and cranial nerves. *IEEE Transactions on Biomedical Engineering* **41**, 567-577, 1994.
[14] Wise KD and Najafi K. Microfabrication techniques for integrated sensors and microsystems. *Science* **29**, 1335-1342, 1991.
[15] Christiansen SH, Singh R, and Gosele U. Wafer Direct Bonding: From Advanced Substrate Engineering to Future Applications in Micro/Nanoelectronics. *Proc IEEE,* **94**, 2060-2106, 2006.